Research Article

Effect of Beam Oscillation Patterns on Laser Welding of 304L Stainless Steel: An Experimental and Modeling Study

Said Ouamer, Asim Iltaf[*] ID **, Noureddine Barka, Shayan Dehghan** ID

Department of Mathematics, Computer Science and Engineering, University of Quebec, Rimouski, QC G5L 3A1, Quebec, Canada
Email: asim.iltaf@uqar.ca

Abstract: Laser welding is increasingly recognized for its precision and efficacy, particularly in handling complex materials like 304L stainless steel. This study investigates the impact of various laser welding parameters, including laser power, welding speed, and beam oscillation patterns (sinusoidal, square, and triangular), on the quality of welded joints. Using the Taguchi method, we structured an L9 experimental design to analyze these parameters systematically. The key findings revealed that beam oscillation patterns significantly influence both the microhardness and tensile strength of the welds. Notably, square and sinusoidal patterns achieved higher microhardness values than triangular patterns, which correlated with their differing impacts on the weld's mechanical properties. Further analysis using analysis of variance (ANOVA) and regression models validated the critical roles of laser power and welding speed, offering predictive insights into optimizing welding conditions for enhanced joint integrity. This study provides a foundational approach for tailoring laser welding settings to improve weld quality in industrial applications, contributing to the body of knowledge with specific data on the effects of beam oscillation in 304L stainless steel welding.

Keywords: laser welding, 304L stainless steel, ANOVA, laser beam oscillations, tensile strength

1. Introduction

Industrial experts agree that laser welding is a significant improvement over friction welding and gas tungsten arc welding because of its superior depth-to-width ratio, smaller heat-affected zone (HAZ), and higher processing efficiency [1]. It has been utilized extensively in several areas, including aerospace manufacturing, the automobile industry, and shipbuilding [2]. Austenitic stainless steel is widely employed in various structural applications due to its good mechanical qualities and economic efficiency [3]. Currently, welded structures constitute a significant proportion of the component assembly [4].

Stainless steel's enhanced corrosion resistance, toughness, aesthetics, and mechanical properties have led to its widespread usage in the construction industry [5]. However, expensive materials and high initial costs make the design less efficient. However, the high starting cost and high cost of materials result in an inefficient design. In contrast to carbon steel, stainless steel does not have a well-defined yield point and exhibits significant strain hardening [6], [7]. Nevertheless, the design provisions are largely based on the perfect elastic-plastic material assumptions, which makes it easier for design engineers to use the new material. However, the widespread use of stainless steel in structural engineering is constrained by the inefficiency of the prevalent design process, which increases structural costs in turn.

The carbon steel design method for stainless steel buildings was validated by accurate experimental and numerical modeling findings reported by Gardner and Nethercot [8], [9], and Young and Lui [10]. In both cases, researchers found that the load-carrying capability of the structural components was underestimated when using the carbon steel design approach. Therefore, Gardner and Theofanous [11] presented new design strategies to make stainless steel structures more efficient.

To effectively address the gaps in the existing literature on beam oscillation in laser welding, this study aims to elucidate the underlying mechanisms by which beam oscillation influences the microstructural and mechanical properties of welded joints. Previous studies have demonstrated the potential of beam oscillation to enhance solidification parameters and modify grain morphology, particularly in high-strength aluminum alloys [12], [13]. However, a comprehensive understanding of the thermal and fluid flow dynamics during beam oscillation remains limited [14], [15]. Additionally, the effect of beam oscillation on dissimilar material welding, which presents unique challenges due to varying thermal properties, has been explored but not exhaustively [16], [17]. The role of beam oscillation in improving weld quality in terms of porosity reduction and microstructure optimization has also been noted in various materials, including ultra-high-strength steels and austenitic stainless steels [18], [19]. Despite these advancements, a research gap persists in quantitatively analyzing how different oscillation patterns and parameters affect the final weld characteristics across different alloys and thicknesses. This research seeks to fill these gaps by conducting a systematic study on the effect of beam oscillation patterns on weld quality, contributing to the optimization of laser welding processes for industrial applications.

Furthermore, Tóth et al. [20] examined the microstructural and mechanical properties of electron-beam-welded super duplex stainless steel, adding to the understanding of welding processes in advanced materials. Yan et al. [21] explored the effects of beam oscillation on microstructural characteristics and mechanical properties in laser-welded steel-copper joints, highlighting significant advancements in this area. Additionally, Mohan et al. [22] presented a sequential modeling approach to determine process capability space during laser welding of high-strength aluminum alloys, contributing valuable insights into the optimization of welding parameters. Tan et al. [23] investigated the impact of beam oscillation frequency on porosity in laser welding of aluminum alloy lap-butt joints, providing crucial data for improving weld quality. Incorporating these studies will provide a robust foundation for identifying and addressing existing research gaps.

This work focuses on austenitic stainless steel 304L, which, according to De Baglion and Mendez [24], is commonly used in the fabrication of nuclear components like reactor vessels and piping systems in pressurized water reactors (PWR). The high corrosion resistance and high weldability make this a popular choice. Hung et al. [25] studied the effect of laser welding modes on the microstructure and mechanical properties of 304L stainless steel components manufactured by laser-foil-printing additive manufacturing [25]. Due to the absence of martensitic structure formation in the HAZ, low-carbon steel alloys rarely necessitate heat treatment either before or after welding. Improved resistance to intergranular stress corrosion cracking makes the low carbon grade the top choice in the nuclear industry.

Studies on the weldability of various stainless steel sheets have found that lowering the amount of heat applied during the welding process is crucial for producing high-quality welds with minimal thermal distortion. Furthermore, only the correct parameters optimize the laser welding [26]-[28]. In the absence of proper welding, the welded joint will be the installation's weak link, affecting its overall performance, quality, durability, and safety [29], [30]. Therefore, the purpose of the current investigation is to analyze the effect of fundamental laser welding parameters, i.e., laser beam power, and welding speed, on three types of oscillation patterns (sinusoidal, square, and triangular).

2. Experimental procedure
2.1 *Materials*

Sheets of stainless steel alloy measuring 1.8 mm × 125 mm × 50 mm were used as the base metal in this study; these sheets were provided by CBR Laser Inc. (Princeville, Quebec). Table 1 displays the material's chemical composition as determined by Energy-dispersive X-ray spectroscopy (EDS), while Table 2 displays its mechanical properties.

**Table 1.** Chemical composition of 304L as measured by EDS (wt%)

Elements	C	Si	Mn	Cr	N	Ni	P	S	Fe
304L	0.11	0.73	5.8	16.5	0.18	4.86	0.035	0.056	Bal.

Table 2. Mechanical properties of 304L

S. No.	Hardness (Hv)	Yield strength (MPa)	Elongation (%)
304L stainless steel	159	210	58

2.2 *Laser beam welding*

The laser source of the welding machine is an IPG Photonics YLS-3000 Yb+: YAG fiber laser operating at 1,070 nm, and the laser head is a BIMO High YAG with a focus diameter of 0.45 mm. Laser welding is a risky process that necessitates the use of an automated workstation; therefore, all welding equipment is mounted on a FANUC robot (Figure 1) [31].

(a) (b)
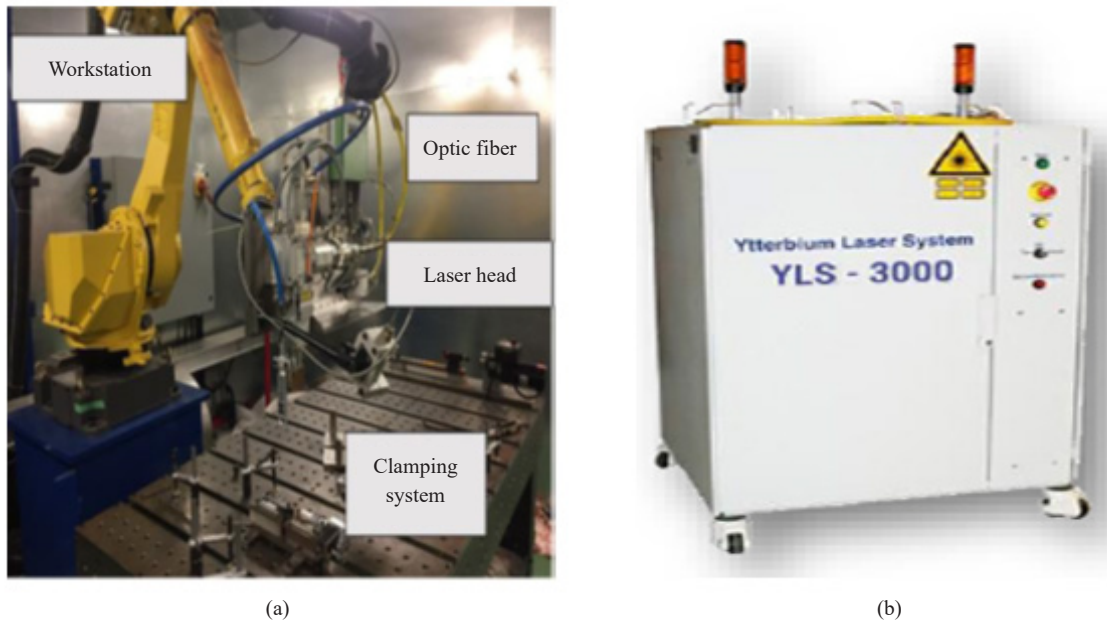
Figure 1. (a) Fanuc®M-710iC robot and HIGHYAG BIMO laser head (b) YLS-3000 laser source

The sheets were laser welded in the butt joint configuration using three types of beam oscillations (sinusoidal, triangular, and square) as shown in Figure 2. For the oscillation of the beam, a DC scanner was used for the three types of beam oscillation at a constant amplitude of 1.5 mm and a constant frequency of 300 Hz. The laser power, welding speed, and welding mode are all adjusted to carry out a series of welds. Taguchi was used to plan the laser welding experiments using an orthogonal L9 grating. This plane was chosen on the basis of the variation of the main welding

parameters, such as laser power, welding speed, and welding mode, as shown in Table 3, which varies between the three levels. The L-9 orthogonal array used for the laser welding tests is shown in Table 4. The selection of laser welding parameters, including laser power, welding speed, and beam oscillation patterns, was methodically planned using the Taguchi method, which is a robust design technique to optimize process parameters efficiently. This approach utilized an L9 orthogonal array, which systematically tested different combinations of these parameters across three levels. This experimental design helps identify the influence of each parameter on the weld quality while minimizing the number of experiments required. The parameters chosen-laser power, welding speed, and the type of beam oscillation (sinusoidal, square, and triangular)-are critical as they directly affect the weld's depth of penetration, fusion zone dimensions, and overall mechanical properties. This study aimed to assess how these variations influence the structural integrity and durability of the welds in 304L stainless steel, ensuring that the process settings optimize the joint quality for practical applications.

Table 3. Process parameter levels

Symbols	M		P	S
	Samples	Level	Laser power (W)	Welding speed (mm/s)
	Sinusoidal	1	1,800	30
	Triangular	2	2,000	40
	Square	3	2,200	50

Table 4. Taguchi L9 orthogonal network

Test No.	Laser power (W)	Welding speed (mm/s)	Welding pattern
1	1,800	50	square
2	1,800	40	sinusoidal
3	1,800	30	triangular
4	2,000	30	sinusoidal
5	2,000	50	triangular
6	2,000	40	square
7	2,200	40	triangular
8	2,200	30	square
9	2,200	50	sinusoidal

2.3 Characterization methods

To obtain specimens for characterization, the welded sheets from each configuration were machined and then cut. The degree of hardness was measured using a Vickers microhardness tester (ST-2000). The microhardness in the fusion zone, defined as a 5-mm measuring line to the right and left of the weld centerline, was determined by placing the polished specimens in a hardness tester. The applied load and dwell time were 200 g and 10 s, respectively.

Welded specimens were subjected to tensile tests at room temperature using an MTS 810 testing machine and the

ASTM E-8 standard, with a constant speed of 0.025 mm/min. To ensure the accuracy of the results, we prepared and tested three samples per experimental series and averaged the results.
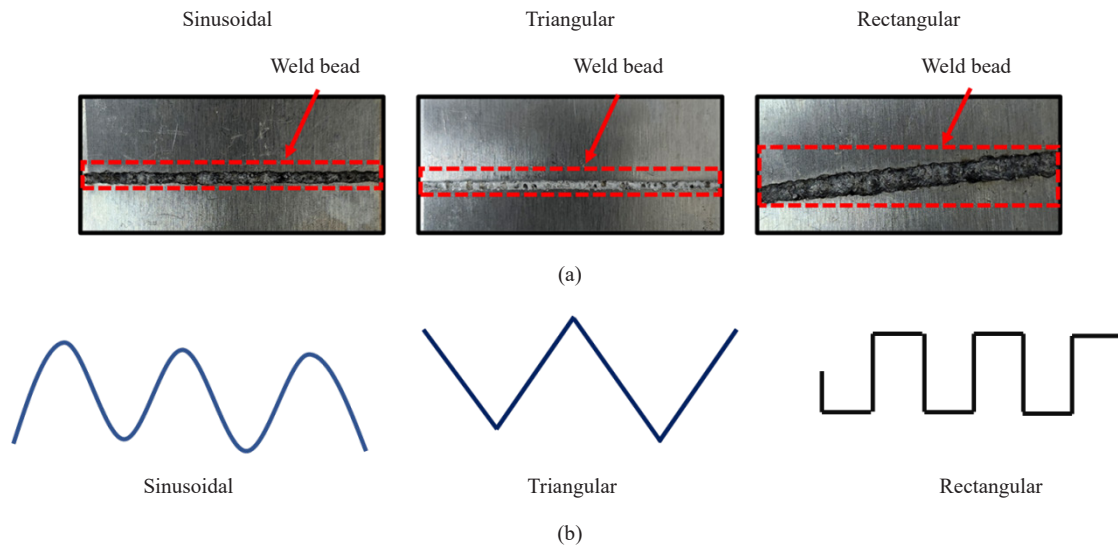
Figure 2. (a) ASIS 304L sheets welded in a butt joint configuration with different oscillation patterns; (b) Schematic representation of the oscillation patterns

2.4 *Analysis of the regression model (ANOVA)*

In this study, ANOVA and regression were used to create mathematical models based on the results of tensile tests performed on specimens welded using three distinct types of laser beam oscillation and varying parameters. Minitab 18 was used for statistical analysis. The significance of the factors and the interactions between them and the responses was calculated using a 95% confidence interval. To create a model that adequately fits the data, insignificant factors and interactions were removed. We used a hierarchical approach to model fitting, which involves excluding variables and their interactions that do not significantly affect the outcome. Similarly, we used regression analysis to develop formulas linking key factors to outcomes. Two-dimensional contours were used to illustrate the correlation between the two continuous factors and the adjusted responses. Main effects plots were used to analyze the influence of different parameter settings on the target mean response.

3. Results and discussion
3.1 *Microhardness*

To assess the mechanical properties of the weldments, microhardness readings were taken in the fusion zone (as depicted in Figure 3). The results show M-shaped hardness distributions for all welding conditions. The maximum hardness values were shown by the square oscillation pattern of the beam, as shown in Figure 3 (a), i.e., ≈ 403 Hv with the parameters (1,800 W, 50 mm/s) and ≈ 382 Hv for the 2,000 W laser power and 40 mm/s welding speed. Additionally, a ≈ 347 Hv value was observed for the 2,200 W laser power and 30 mm/s welding speed. The maximum hardness values for the samples welded by triangular beam oscillation as shown in Figure 3 (b) were about ≈ 327 Hv with parameters (2,000 W, 50 mm/s) and about ≈ 300 Hv with parameters (2,200 W, 40 mm/s). Furthermore, a ≈ 237 Hv value can be observed with parameters (1,800 W, 30 mm/s). The maximum hardness values for the specimens welded by sinusoidal beam oscillation are shown in Figure 3 (c), i.e., ≈ 362 Hv with parameters (2,200 W, 50 mm/s) and ≈ 341 Hv with parameters (1,800 W, 40 mm/s). Moreover, ≈ 320 Hv with parameters (2,000 W, 30 mm/s). The details are presented

in Table 5. It can be seen that the maximum microhardness values of sinusoidal beam oscillation and square beam oscillation laser welding are higher than those of triangular oscillation patterns. The microhardness measurements, taken across the fusion zones of the welds, showed distinctive M-shaped hardness distributions for each welding condition, indicative of varying thermal effects across the weld area. Notably, the welds executed with the square oscillation pattern exhibited the highest microhardness values, peaking at approximately 403 Hv with a laser power of 1,800 W laser power and a welding speed of 50 mm/s. This was followed by the sinusoidal oscillation pattern, which showed a maximum hardness of approximately 362 Hv using the 2,200 W and 50 mm/s settings. The triangular pattern resulted in comparatively lower hardness values, with a peak around 327 Hv at 2,000 W and 50 mm/s. These trends suggest that the square and sinusoidal patterns are more effective in achieving higher hardness, potentially due to better energy distribution and heat input control, leading to a more refined microstructure in the fusion zone. The triangular pattern, which produces the lowest hardness, might indicate less optimal heat distribution or faster cooling rates, affecting the microstructural transformations beneficial for higher hardness.


(a)

(b)

(c)
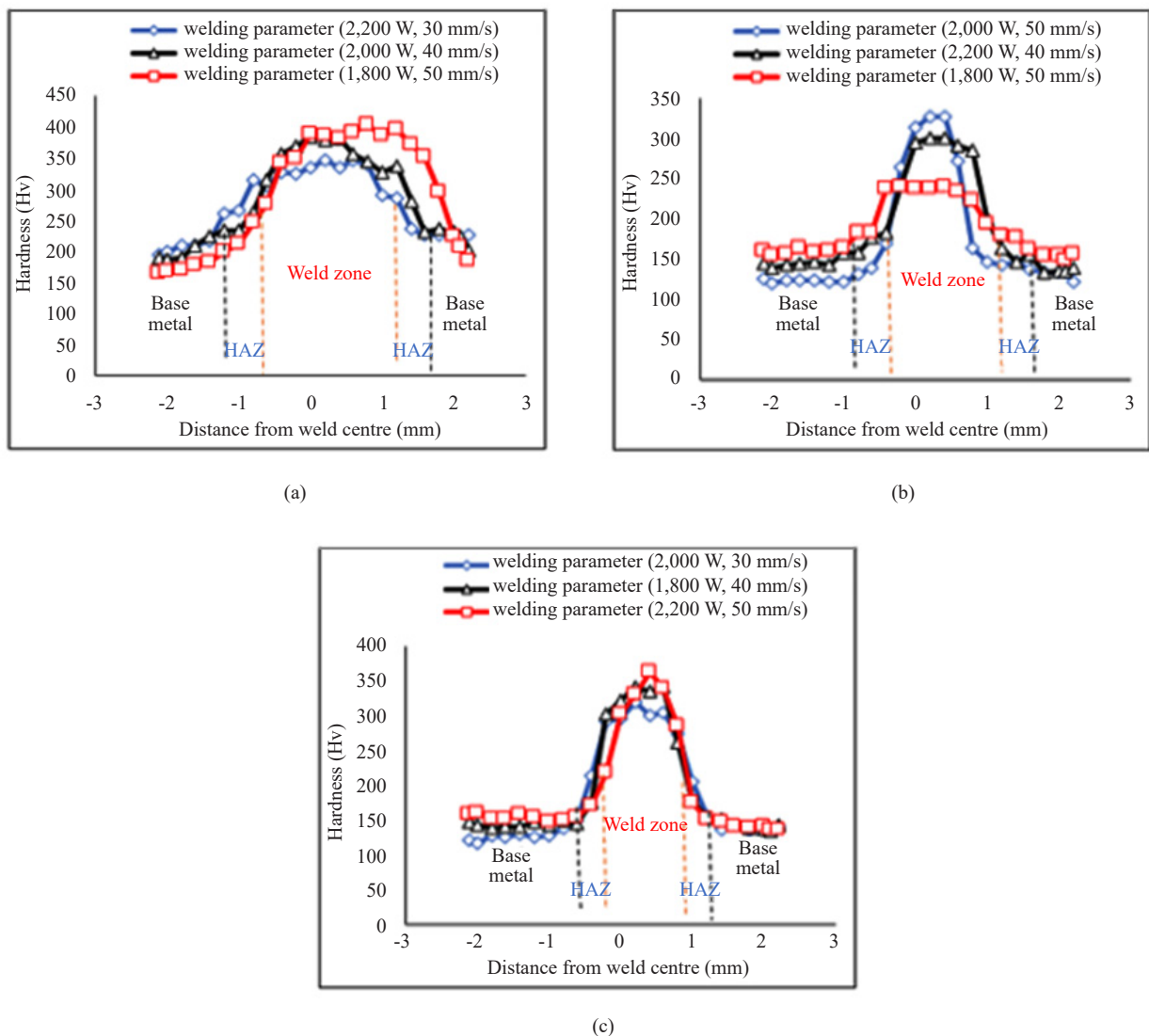
Figure 3. The hardness distributions for all the welded samples with different parameters: (a) Square pattern, (b) Triangular pattern, and (c) Sinusoidal pattern

Table 5. Microhardness values of the welded samples

Laser power (W)	Welding speed (mm/s)	Pattern	Microhardness (Hv)	FZ width (mm)	FZ penetration
1,800	50	Square	403 ± 3.7	2.1	Full
1,800	40	Sinusoidal	341 ± 5.3	1.4	Full
1,800	30	Triangular	237 ± 2.6	1.7	Full
2,000	30	Sinusoidal	320 ± 5.3	1.4	Full
2,000	50	Triangular	327 ± 2.6	1.7	Full
2,000	40	Square	382 ± 3.7	2.1	Full
2,200	40	Triangular	300 ± 2.6	1.7	Full
2,200	30	Square	347 ± 3.7	2.1	Full
2,200	50	Sinusoidal	362 ± 5.3	1.4	Full

3.2 *Tensile tests*

Tensile strength results were obtained for all welding conditions. Figure 4 depicts the results of the tests, which showed that all of the samples broke away from the fusion zone and the heat-affected zone, directly into the base metal. Figure 5 shows the stress-strain curves for the welded specimens. The results were found to be in the range of 345.25 to 366.26 MPa as shown in Table 6. The results showed that all samples fractured outside the fusion zone, indicating that the welds were strong enough to ensure that failure occurred in the base material, which is a positive indication of weld quality. Among the oscillation patterns, the triangular pattern achieved the highest UTS of 366.26 MPa with a laser power of 1,800 W laser power and a welding speed of 30 mm/s. In contrast, the lowest UTS recorded was 345.25 MPa for the triangular pattern at 2,000 W and 50 mm/s. This suggests that while the triangular pattern can reach high strength under certain conditions, its performance might be more sensitive to variations in welding speed and power. The sinusoidal and square patterns displayed more consistent, albeit slightly lower, UTS values across the tested ranges. These findings indicate that the choice of beam oscillation pattern, along with the adjustment of laser power and welding speed, critically influences the tensile strength of the weld, with the triangular pattern offering the potential for high strength but possibly requiring more precise control over welding conditions to optimize results.
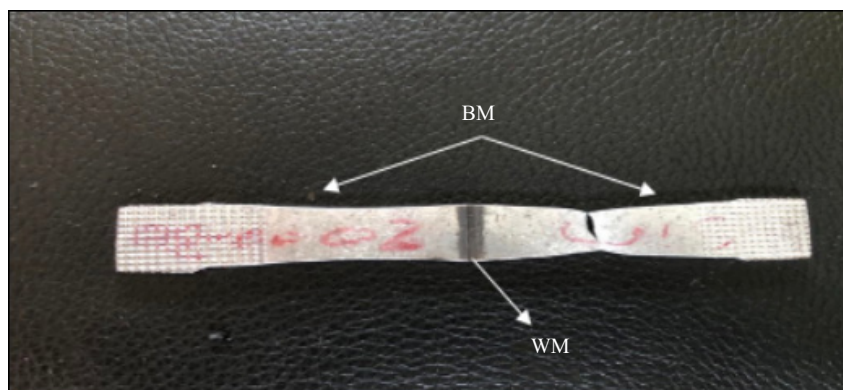
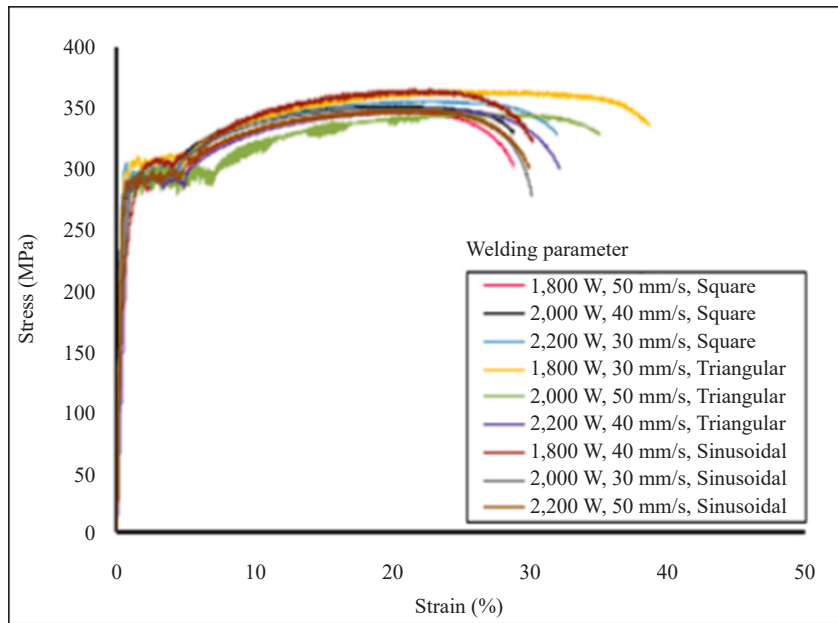**Figure 4.** Top view of the fractured sample after the tensile test

Figure 5. Stress-strain curves for all specimens

Table 6. UTS values of the welded samples

S. No.	Laser power (W)	Welding speed (mm/s)	Pattern	UTS (MPa)
1	1,800	50	Square	361.51 ± 2.7
2	1,800	40	Sinusoidal	364.50 ± 4.8
3	1,800	30	Triangular	366.26 ± 5.5
4	2,000	30	Sinusoidal	350.50 ± 4.1
5	2,000	50	Triangular	345.25 ± 6.1
6	2,000	40	Square	349.16 ± 2.1
7	2,200	40	Triangular	347.88 ± 6.5
8	2,200	30	Square	350.66 ± 2.8
9	2,200	50	Sinusoidal	349.24 ± 4.5

The parametric combination of experimental cycle 5 in the welding scheme demonstrates a low tensile strength value of 345.25 MPa (see Table 5). Contrarily, the maximum tensile strength is calculated as 366.26 MPa via the parametric combination of experimental cycle 3 in the welding scheme. The UTS value rises from parametric combinations 5 to 3, even though the welding mode factor remains the same. According to the results, the influence of the welding mode factor on the tensile strength is negligible. However, the welding power and welding speed are two other variables that have a major impact on the shift in the tensile strength value.

Figure 6 shows scanning electron microscopy (SEM) images of the fractured surface after tensile testing. All the weldments fractured in a "cup and cone" way, hence this figure is representative of all the weldments. Cup-and-cone fractures are caused by microvoid coalescence and are characteristic of ductile fracture mechanisms. However, Figure 6

also shows some cleavage facets that indicate a brittle fracture in some regions of the weldments. Therefore, the overall fracture mode was dominantly ductile along with minor brittle fractures in certain areas of the weldments.
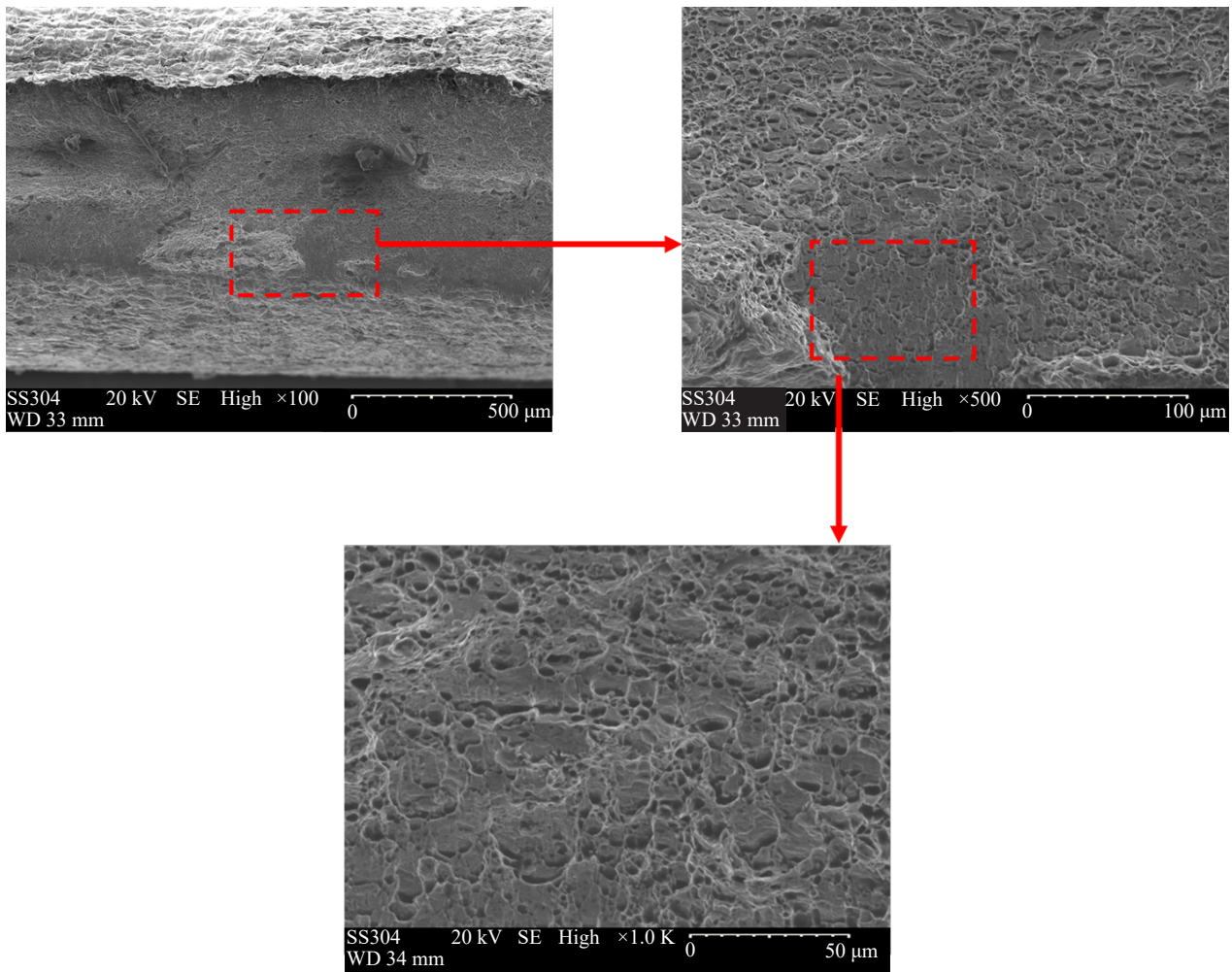

Figure 6. SEM images of the fractured surface of the tensile sample

3.3 Statistical models and analysis

The appropriate response model for these response factors was selected based on the summaries of the experimental results.

3.3.1 Analysis of variance (ANOVA)

ANOVA was used to determine the relative importance of each experimental parameter through statistical analysis. By comparing the square of the results to a calculated approximation of the experimental errors at predetermined levels of confidence, ANOVA formally tests the findings of all the principal factors and their relationships [32]. Tables 7-8 show the results obtained by ANOVA for the tensile strength. About 65.95% of the calculated percentage is attributable to the welding power (W), followed by the welding speed (mm/s) at 4.32% and the welding mode at 0.81%. The effects of the bidirectional interactions were also examined, and it was found that the interaction (P * P) ranks first, contributing more than $ 28.03%. The interaction (P * S) with a smaller contribution of 0.89% occupies the second rank. All the P values are lower than 0.05, so we know that all the variables are significant.

Table 7. ANOVA results for the interaction model

Variable	DDL	Square sum	Contribution (%)	Medium square	F-value	P-value
Model	6	499.305	99.99	83.217	3,324.26	0.000
Power (W)	1	329.3	65.95	156.802	6,263.75	0.000
Speed (mm/s)	1	21.584	4.32	5.624	224.65	0.004
pattern	2	4.033	0.81	2.884	115.2	0.009
Two-factor interaction: P * P	1	139.946	28.03	139.946	5,590.4	0.000
Two-factor interaction: P * S	1	4.44	0.89	4.44	177.37	0.006
Error	2	0.05	0.01	0.025		
Total	8	499.355	100			

S	R-sq	R-sq (adj)	PRESS	R-sq (pred)
0.158219	99.99%	99.96%	0.947424	99.81%

Table 8. Coefficient of the bidirectional interaction model

Term	Coefficient	P value
Constant	1,326.1	0.000
P	-0.9033	0.000
S	-1.680	0.004
M	-	-
Square	0.890	0.014
Sinusoidal	0.3700	0.047
Triangular	-1.2600	0.004
P * P	0.000209	0.000
P * S	0.000745	0.006

It is clear from Tables 6 and 7 that the developed models are quite precise and can be used for further analysis. The following are the final mathematical models derived from the coded factors using Minitab:

$$\text{Square Pattern UTS} = 1{,}327.0 - 0.9033\,P - 1.680\,S + 0.000209\,P \times P + 0.000745\,P \times S \qquad (1)$$

$$\text{Sinusoidal Pattern UTS} = 1{,}326.4 - 0.9033\,P - 1.680\,S + 0.000209\,P \times P + 0.000745\,P \times S \qquad (2)$$

$$\text{Triangular Pattern UTS} = 1{,}324.8 - 0.9033\,P - 1.680\,S + 0.000209\,P \times P + 0.000745\,P \times S \qquad (3)$$

Validation of statistical models typically involves ensuring that the residuals are normally distributed. In a well-

fitting model, the residuals (the gaps between the predicted and observed responses) should have a zero-mean normal distribution. For the most part, when conducting a regression analysis, the least squares approach is chosen. A perfect scenario would result in a straight line with no deviations [33], [34]. A normal residue plot for the weld fill passes, weld bead width, and bead integrity is shown in Figure 7. The majority of the points, with a few exceptions, lie on or very close to the straight line, demonstrating the accuracy of the models.
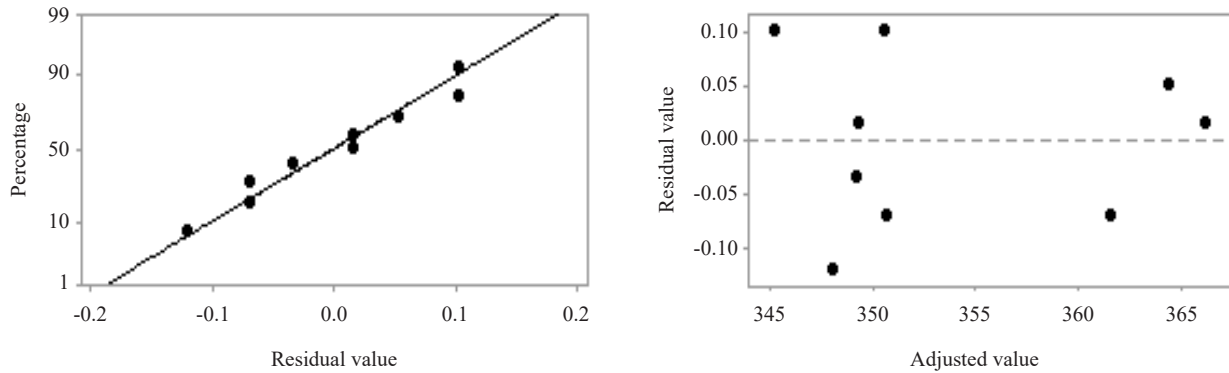
Figure 7. Residual plots for each model

3.3.2 *Variation of the developed model*

To ensure that the developed models were sufficient, predicted values were calculated for all 9 experimental series and they were compared with the measured experimental values. The experiment setup, observed data, predicted values, and percentage of error are all summarised in Table 9. The percentages of error in the prediction also agree well with the experimental results, demonstrating the high level of accuracy of the developed models. In Figure 8, we see a scatter plot of the fitted values versus the measured values. As the figures show, the residuals in the prediction of each response are small and cluster around the diagonal, suggesting that the developed models are sufficient.

**Table 9.** Confirmation experiments

| S. No.	Laser power (W)	Welding speed (mm/s)	Pattern type	Ultimate tensile strength (UTS) value (MPa)		Error (%)
				Experimental	Model predicted	
1	1,800	50	Square	361.51	361.27	0.07
2	1,800	40	Sinusoidal	364.5	364.06	0.12
3	1,800	30	Triangular	366.26	365.85	0.11
4	2,000	30	Sinusoidal	350.5	350.1	0.11
5	2,000	50	Triangular	345.25	344.7	0.16
6	2,000	40	Square	349.16	348.8	0.1
7	2,200	40	Triangular	347.88	347.6	0.12
8	2,200	30	Square	350.66	350.07	0.17
9	2,200	50	Sinusoidal	349.24	348.65	0.17
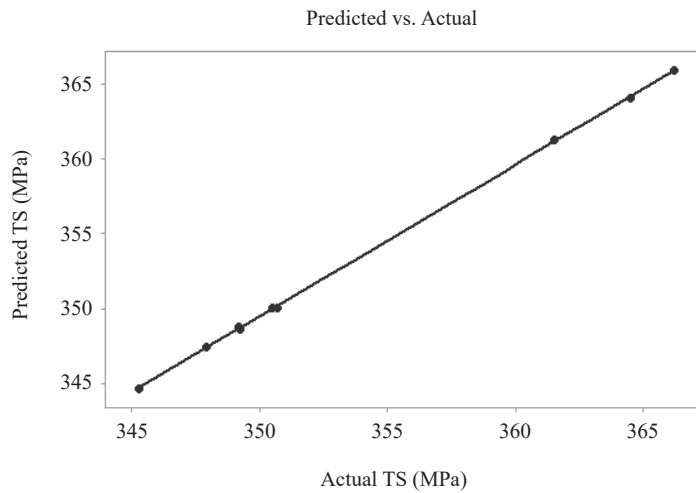
Figure 8. Comparison of measured values with fitted values for the model

## 3.4 *Effects of process parameters on UTS response*

The main process parameter effects on the UTS values of the welded specimens are plotted in Figure 9. Note that these plots illustrate the averages of the data as a function of the factor level. Based on these effects, each factor can be evaluated graphically. Laser power and welding speed were found to have the greatest impact on the mechanical properties of the welded specimens, whereas beam oscillation played a secondary role.
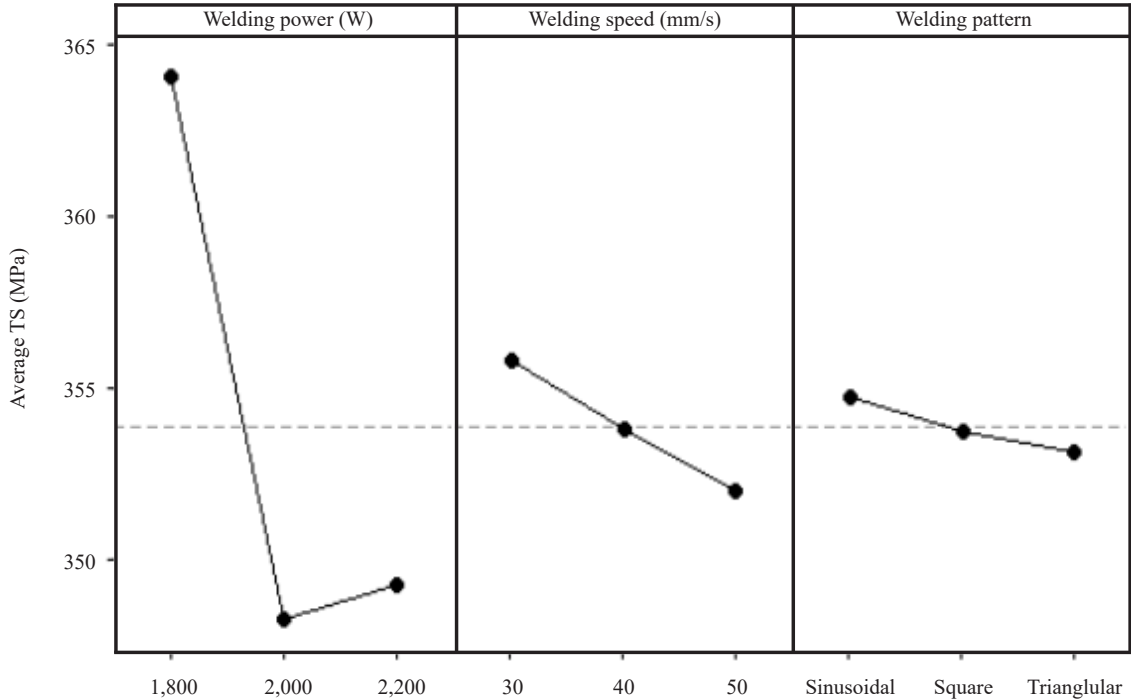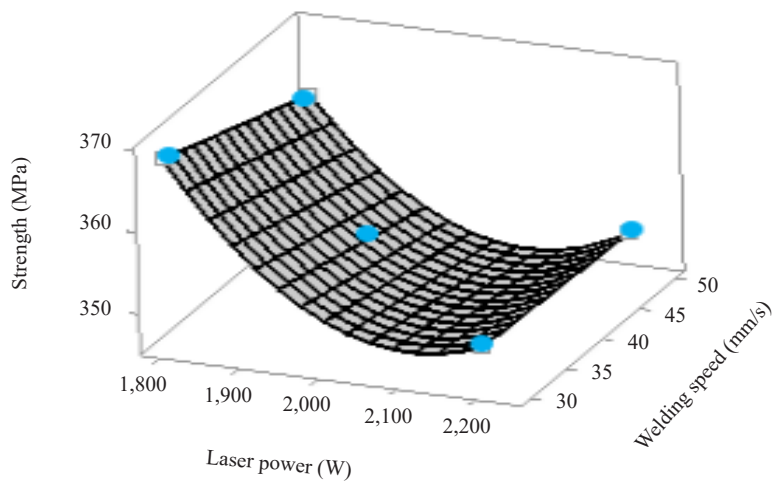

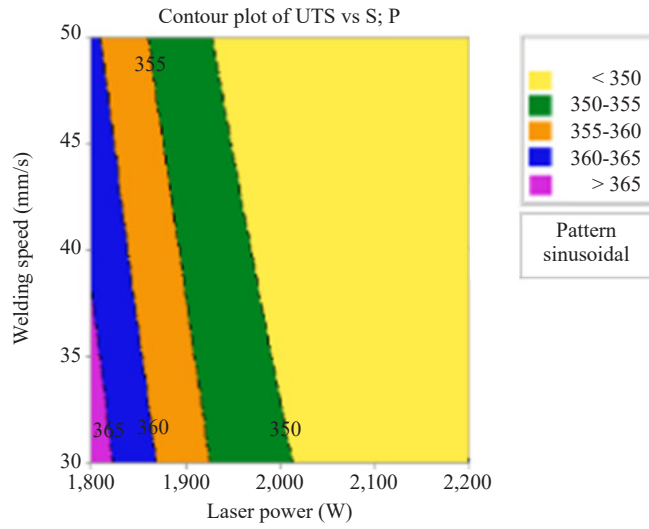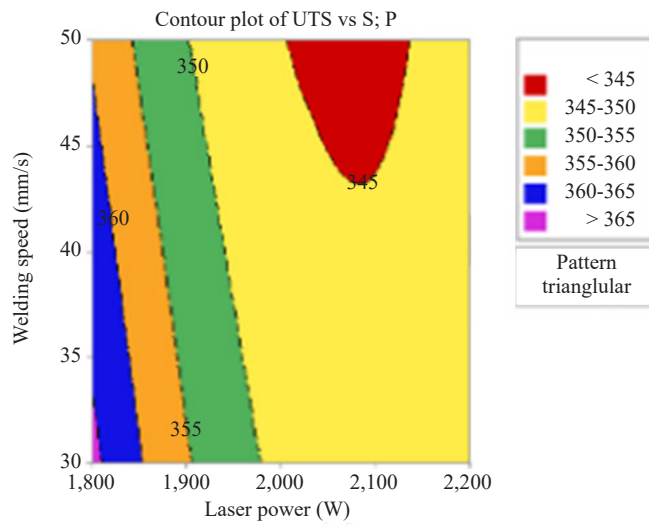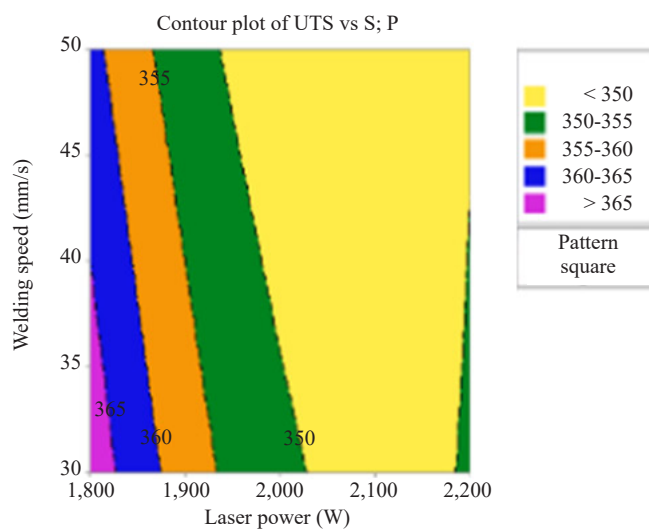Figure 9. Graph depicting the main effects on the UTS response
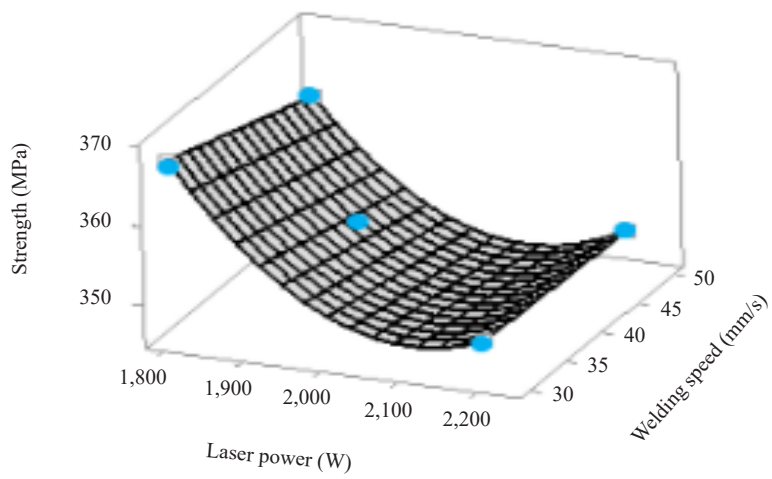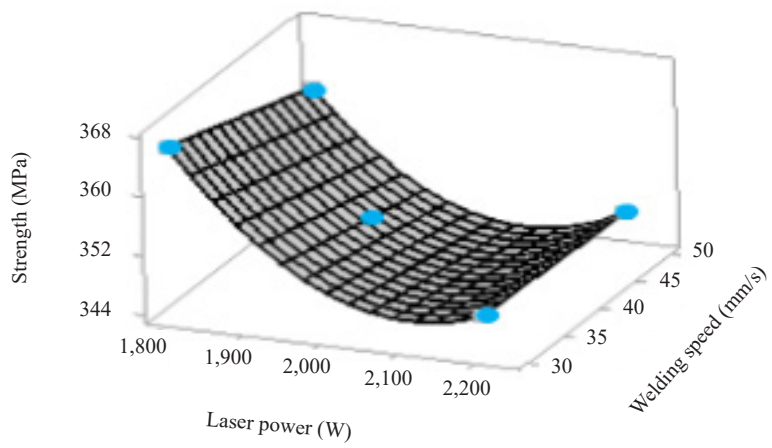
Figure 10. Surface diagrams of UTS (a) sinusoidal trajectory, (b) triangular trajectory, and (c) square trajectory

Figure 11. Contour plots of UTS during welding of the three oscillation patterns (sinusoidal, triangular, and square)

Figure 10 depicts the combined influences of laser power and welding speed on the tensile strength for the sinusoidal, triangular, and square oscillation patterns. At high welding rates and with a strong laser, we find that the weld resistance is minimal. The strength of the joint was improved by reducing the laser power and welding speed, which led to more melting and mixing at the joint. According to Figure 10, the values of tensile strength that are of interest are those above 360 MPa. These values are located in the blue and pink regions. The optimum response of tensile strength is obtained with a laser power of 1,800 W and a welding speed in the range of 30-40 mm/s with a sinusoidal oscillation pattern, as shown in Figure 11. It has a slightly higher tensile value than the other models. Therefore, we can conclude that the most suitable combination of welding parameters could be a laser power of 1,800 W, a welding speed in the 30-40 mm/s range, and a sinusoidal laser welding pattern.

3.5 *UTS optimization using desirability function analysis*

One of the most common practices for improving product quality is analyzing preferences using a desirability function. In this optimization, we aim to achieve a tensile strength (UTS) of 368.35 MPa, which is the ideal value for a strong weld. The preferred outcome was achieved by setting the linear desirability function's lower bound, target, and upper bound to equal values. It was assumed that the linear desirability function (d) had a value of 1. The optimization feature in Minitab v17 looks for a set of factor levels that meets the criteria for all answers and all factors at the same time. This method of optimization uses a mathematical model to explore the design space and identify the factors and their optimum settings. Standard optimization criteria have been used in this investigation. UTS at 368.35 MPa was chosen as the target in the criterion, with all other process parameters being held constant. The UTS optimization curves are shown in Figure 12. Each row of this graph represents a response variable, and each column represents a process parameter. From the optimization graph (Figure 12), we can infer that the laser power of 1,800 W, the welding speed of 30 mm/s, and the square pattern of laser welding are optimal for a response of 368.35.
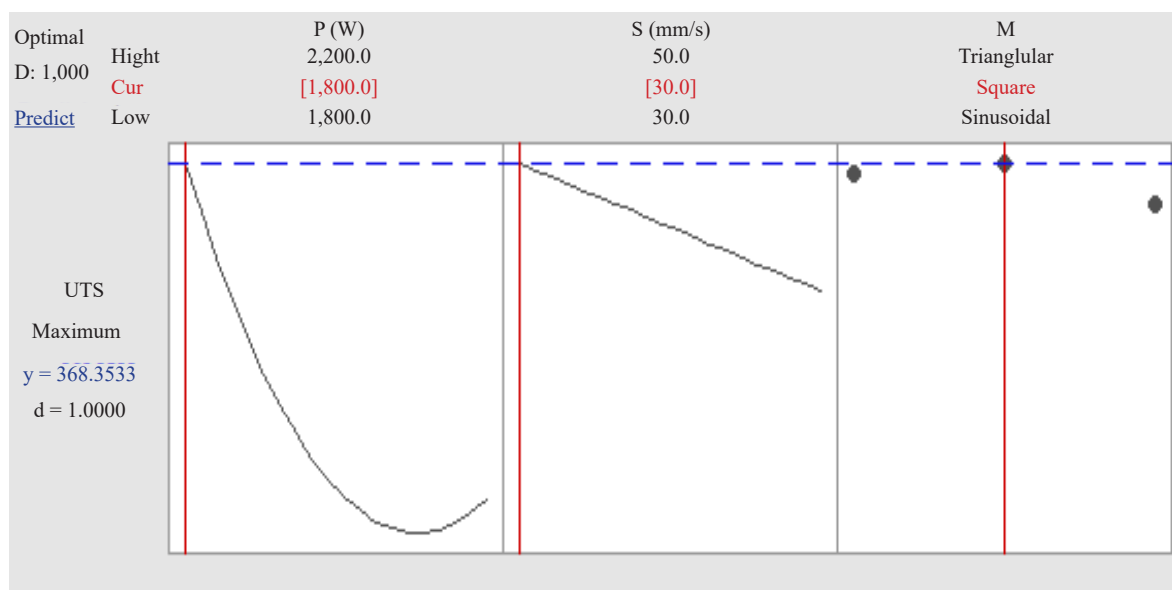

Figure 12. UTS response optimization diagram

4. Conclusions

The following conclusions can be drawn from the current study:
• The microhardness of all samples reaches its maximum in the fusion zone and gradually decreases from the fusion zone towards the base metal. The maximum microhardness values were achieved for the sinusoidal and square

oscillation patterns.

• Using experimental and modeling data, it was determined that laser power and welding speed are critical parameters that significantly affect the mechanical properties of the welded joints. Despite this, beam oscillation does impact the UTS values of the weldments, albeit only slightly.

• The optimum combination of welding parameters for the current study was identified to be: 1,800 W laser power, 30-40 mm/s welding speed, and sinusoidal oscillation pattern.

• To achieve the desired UTS value, i.e., 368.35 MPa, the optimal combination of welding parameters was identified to be: 1,800 W laser power, 30 mm/s welding speed, and a square oscillation pattern.

Conflict of interest

The authors declare that they have no known competing financial interests or personal relationships that could have appeared to influence the work reported in this paper.

References

[1] K. Hu, W. Muneer, J. Zhang, and X. Zhan, "Effect of beam oscillating frequency on the microstructure and mechanical properties of dissimilar laser welding of AA2060 and AA6061 alloy," *Materials Science and Engineering: A*, vol. 832, pp. 142431, 2022.

[2] T. Yan, J. Liu, K. Hu, X. Kang, and X. Zhan, "Microstructure and texture evolution of Ti-6Al-4V alloy T-joint fabricated by dual laser beam bilateral synchronous welding," *Materials Science and Engineering: A*, vol. 822, pp. 141426, 2021.

[3] W. Yang, J. Xin, C. Fang, W. Dai, J. Wei, J. Wu, and Y. Song, "Microstructure and mechanical properties of ultra-narrow gap laser weld joint of 100 mm-thick SUS304 steel plates," *Journal of Materials Processing Technology*, vol. 265, pp. 130-137, 2019.

[4] K. Mao, H. Wang, Y. Wu, V. Tomar, and J. P. Wharry, "Microstructure-property relationship for AISI 304/308L stainless steel laser weldment," *Materials Science and Engineering: A*, vol. 721, pp. 234-243, 2018.

[5] L. Gardner, "Stability and design of stainless steel structures - Review and outlook," *Thin-Walled Structures*, vol. 141, pp. 208-216, 2019.

[6] I. Arrayago, E. Real, and L. Gardner, "Description of stress-strain curves for stainless steel alloys," *Materials & Design*, vol. 87, pp. 540-552, 2015.

[7] L. Gardner and X. Yun, "Description of stress-strain curves for cold-formed steels," *Construction and Building Materials*, vol. 189, pp. 527-538, 2018.

[8] L. Gardner and D. A. Nethercot, "Experiments on stainless steel hollow sections-Part 1: Material and cross-sectional behaviour," *Journal of Constructional Steel Research*, vol. 60, no. 9, pp. 1291-1318, 2004.

[9] L. Gardner and D. A. Nethercot, "Experiments on stainless steel hollow sections-Part 2: Member behaviour of columns and beams," *Journal of Constructional Steel Research*, vol. 60, no. 9, pp. 1319-1332, 2004,

[10] B. Young and W.-M. Lui, "Behavior of cold-formed high strength stainless steel sections," *Journal of Structural Engineering*, vol. 131, no. 11, pp. 1738-1745, 2005.

[11] L. Gardner and M. Theofanous, "Discrete and continuous treatment of local buckling in stainless steel elements," *Journal of Constructional Steel Research*, vol. 64, no. 11, pp. 1207-1216, 2008.

[12] A. Mohan, D. Ceglarek, P. Franciosa, and M. Auinger, "Numerical study of beam oscillation and its effect on the solidification parameters and grain morphology in remote laser welding of high-strength aluminium alloys," *Science and Technology of Welding and Joining*, vol. 28, no. 5, pp. 362-371, 2023.

[13] C. Hagenlocher, M. Sommer, F. Fetzer, R. Weber, and T. Graf, "Optimization of the solidification conditions by means of beam oscillation during laser beam welding of aluminum," *Materials & Design*, vol. 160, pp. 1178-1185, 2018.

[14] A. Mohan, D. Ceglarek, and M. Auinger, "Numerical modelling of thermal quantities for improving remote laser welding process capability space with consideration to beam oscillation," *International Journal of Advanced Manufacturing Technology*, vol. 123, no. 3-4, pp. 761-782, 2022.

[15] T. Liu, Z. Mu, R. Hu, and S. Pang, "Sinusoidal oscillating laser welding of 7075 aluminum alloy: Hydrodynamics,

porosity formation and optimization," *International Journal of Heat and Mass Transfer*, vol. 140, pp. 346-358, 2019.

[16] A. Mohan, P. Franciosa, D. Ceglarek, and M. Auinger, "Numerical simulation of transport phenomena and its effect on the weld profile and solute distribution during laser welding of dissimilar aluminium alloys with and without beam oscillation," *International Journal of Advanced Manufacturing Technology*, vol. 124, no. 10, pp. 3311-3325, 2023.

[17] H. Ramiarison, N. Barka, F. Mirakhorli, F. Nadeau, and C. Pilcher, "Parameter optimization for laser welding of dissimilar aluminum alloy: 5052-H32 and 6061-T6 considering wobbling technique," *International Journal of Advanced Manufacturing Technology*, vol. 118, no. 11-12, pp. 4195-4211, 2022.

[18] C. Chen, W. Wang, D. Li, Y. Cai, Y. Zhang, and K. Zhang, "Effect of beam oscillation on microstructure and properties of laser-TIG hybrid welding of D406A ultra-high strength steel," *Journal of Manufacturing Processes*, vol. 57, pp. 798-805, 2020.

[19] K. Hao, G. Li, M. Gao, and X. Zeng, "Weld formation mechanism of fiber laser oscillating welding of austenitic stainless steel," *Journal of Materials Processing Technology*, vol. 225, pp. 77-83, 2015.

[20] T. Tóth, A. C. Hesse, V. Kárpáti, V. Mertinger, and K. Dilger, "Microstructural and mechanical properties of electron beam welded super duplex stainless steel," *Welding in the World*, pp. 1-12, 2024.

[21] F. Yan, Y. Qin, B. Tang, Y. Zhou, Z. Gao, Y. Hu, C. Hu, Z. Xiao, Z. Xiao, and C. Wang, "Effects of beam oscillation on microstructural characteristics and mechanical properties in laser welded steel-copper joints," *Optics & Laser Technology*, vol. 148, pp. 107739, 2022.

[22] A. Mohan, Q. Hayat, S. K. Dinda, V. V. Pamarthi, P. Franciosa, D. Ceglarek, and M. Auinger, "A sequential modelling approach to determine process capability space during laser welding of high-strength Aluminium alloys," *Journal of Advanced Joining Processes*, vol. 9, pp. 100218, 2024.

[23] Z. Tan, Z. Zhang, F. Liu, X. Qin, X. Zhou, P. Gao, T. Yu, and C. Tan, "Effect of beam oscillation frequency on porosity in laser welding of aluminum alloy lap-butt joints," *Science and Technology of Welding and Joining*, vol. 29, no. 2, pp. 124-133, 2024.

[24] L. De Baglion and J. Mendez, "Low cycle fatigue behavior of a type 304L austenitic stainless steel in air or in vacuum, at 20 °C or at 300 °C: Relative effect of strain rate and environment," *Procedia Engineering*, vol. 2, no. 1, pp. 2171-2179, 2010.

[25] C. H. Hung, W. T. Chen, M. H. Sehhat, and M. C. Leu, "The effect of laser welding modes on mechanical properties and microstructure of 304L stainless steel parts fabricated by laser-foil-printing additive manufacturing," *International Journal of Advanced Manufacturing Technology*, vol. 112, no. 3-4, pp. 867-877, 2021.

[26] Z. Tian, Y. Peng, L. Zhao, H. Xiao, and C. Ma, "Study of weldability of high nitrogen stainless steel," in: *Advanced Steels*, Y. Weng, H. Dong, and Y. Gan, Eds. Berlin, Heidelberg: Springer, 2011, pp. 465-473.

[27] L. Li, "The advances and characteristics of high-power diode laser materials processing," *Optics and Lasers in Engineering*, vol. 34, no. 4-6, pp. 231-253, 2000.

[28] A. Kurc-Lisiecka and A. Lisiecki, "Laser welding of the new grade of advanced high-strength steel Domex 960," *Materials and Technology*, vol. 51, no. 2, pp. 199-204, 2017.

[29] A. Kurc-Lisiecka, "Impact toughness of laser-welded butt joints of the new steel grade strenx 1100MC," *Materials and Technology*, vol. 51, no. 4, pp. 643-649, 2017.

[30] A. Kurc-Lisiecka and A. Lisiecki, "Weld metal toughness of autogenous laser-welded joints of high-strength steel DOMEX 960," *Materials Performance and Characterization*, vol. 8, no. 6, pp. 1226-1236, 2019.

[31] S. Katayama, "Introduction: fundamentals of laser welding," *Handbook of Laser Welding Technologies*, Sawston, UK: Woodhead Publishing; 2013, pp. 3-16.

[32] N. H. M. Nor, N. Muhamad, M. H. I. Ibrahim, M. Ruzi, and K. R. Jamaladin, "Optimization of injection molding parameter of Ti-6Al-4V powder mix with palm stearin and polyethylene for the highest green strength by using taguchi method," *International Journal of Mechanical and Materials Engineering*, vol. 6, no. 1, pp. 126-132, 2011.

[33] H. Shi, K. Zhang, Z. Xu, T. Huang, L. Fan, and W. Bao, "Applying statistical models optimize the process of multi-pass narrow-gap laser welding with filler wire," *The International Journal of Advanced Manufacturing Technology*, vol. 75, no. 1, pp. 279-291, 2014.

[34] M. M. A. Khan, L. Romoli, M. Fiaschi, G. Dini, and F. Sarri, "Multiresponse optimization of laser welding of stainless steels in a constrained fillet joint configuration using RSM," *The International Journal of Advanced Manufacturing Technology*, vol. 62, no. 5, pp. 587-603, 2012.